

Magnetic and collective rotation in ^{79}Br

R. Schwengner,¹ F. Dönau,¹ T. Servene,¹ H. Schnare,¹ J. Reif,¹ G. Winter,^{1,*} L. Käubler,¹ H. Prade,¹ S. Skoda,^{1,2} J. Eberth,² H. G. Thomas,² F. Becker,² B. Fiedler,² S. Freund,² S. Kasemann,² T. Steinhardt,² O. Thelen,² T. Härtlein,³ C. Ender,³ F. Köck,³ P. Reiter,^{3,†} and D. Schwalm³

¹*Institut für Kern- und Hadronenphysik, Forschungszentrum Rossendorf, D-01314 Dresden, Germany*

²*Institut für Kernphysik, Universität zu Köln, D-50937 Köln, Germany*

³*Max-Planck-Institut für Kernphysik, D-69117 Heidelberg, Germany*

(Received 17 January 2002; published 4 April 2002)

Excited states of the nucleus ^{79}Br were investigated via the reaction $^{76}\text{Ge}(^{7}\text{Li},4n)$ at a beam energy of 35 MeV. Coincidence data of emitted γ rays were measured with an arrangement of six EUROBALL CLUSTER detectors. The $E2$ bands built on the $9/2^+$ and $3/2^-$ states were extended up to $J=37/2$ at $E\approx 8.8$ MeV. The $M1$ band starting with a $15/2^-$ state at 2.6 MeV was observed up to $J=(29/2)$ at $E=6.4$ MeV. Crossover $E2$ transitions within this band were observed for the first time. Mean lifetimes of 17 levels were deduced using the Doppler-shift-attenuation method. The $M1$ band can be described within the tilted-axis-kranking model on the basis of the tilted three-quasiparticle configuration $\pi(g_{9/2}) \nu(g_{9/2}) \nu(fp)$ which has a triaxial shape. This band appears as a mixed case including contributions of both magnetic and collective rotation.

DOI: 10.1103/PhysRevC.65.044326

PACS number(s): 23.20.En, 23.20.Lv, 27.50.+e

I. INTRODUCTION

Magnetic rotation [1], a novel rotational mode first described in the tilted-axis cranking (TAC) model [2,3], is predicted to occur in weakly deformed nuclei ($\epsilon_2 \leq 0.15$) for multiquasiparticle configurations. Few protons occupy orbitals with long spin vectors above a closed shell (high- j particlelike orbitals) while neutrons fill up a shell except for a few holes (high- j holelike orbitals), or vice versa. Since in this case the perpendicular coupling of the proton and neutron spins is energetically favored, a substantial component of the magnetic dipole moment perpendicular to the total spin is produced. This gives rise to strong $M1$ transitions with strengths up to several μ_N^2 within such a rotational band. These $M1$ transition strengths decrease gradually with increasing spin due to the gradual alignment of the particle spins parallel to the direction of the total spin, which is called shears mechanism [1,4,5]. Because of the small deformation the $E2$ transitions are rather weak and therefore the notion of magnetic rotation is used to distinguish those bands from the usual rotational mode with strong electric quadrupole transitions. The ratios of the transition strengths are typically in the order of $B(M1)/B(E2) \approx 20-40$ ($\mu_N/e\text{b}$)² in these magnetic bands and decrease with increasing spin [6]. Evidence of magnetic rotation was found for the first time in nearly spherical nuclei around ^{200}Pb [4,7–12]. The regular dipole sequences with rotational-like level energies $E \propto J(J+1)$, i.e., $E_\gamma(\Delta J=1) \propto J$, evolving at high spin J are in striking contrast to the multipletlike irregular level scheme observed in these nuclei at low spin.

Magnetic rotation was predicted for several mass regions near shell closures [13]. Indeed, shears bands were observed in nuclei around $A=110$ [14–18] and $A=140$ [19]. Re-

cently, we found regular $M1$ bands including ratios of $B(M1)/B(E2) \approx 25$ ($\mu_N/e\text{b}$)² in the doubly odd nuclei ^{82}Rb ($N=45$) and ^{84}Rb ($N=47$) [20,21]. These bands were well described in the TAC model on the basis of a four-quasiparticle ($4qp$) configuration and they can be considered as the first evidence of magnetic rotation in the mass $A=80$ region.

The shears mechanism of the magnetic rotation is, however, not the only way to create level sequences connected by strong $M1$ transitions. In the mass $A=80$ region bands with large $M1$ strengths of $B(M1) \leq 1.8 \mu_N^2$ are well known in several odd-mass nuclei. They were discovered for the first time in ^{81}Kr and have been explained on the basis of a semiclassical coupling scheme for the spins of the involved unpaired particles [22]. Indications of similar $M1$ sequences were also observed in the odd- N nuclei $^{79,83}\text{Kr}$ [23,24], ^{83}Sr [25], and in the odd- Z nuclei $^{77,79,81}\text{Br}$ [26–28], and $^{79,81,83,85}\text{Rb}$ [29–32]. However, the character of the $M1$ sequences observed in nuclei with $N \leq 44$ is expected to be somewhat different as compared with magnetic rotation due to the large quadrupole deformation of $\epsilon_2 \approx 0.20-0.25$ involved. In these nuclei rotational bands are built on the ground state or on low-lying states and manifest their collective character by predominating stretched ($\Delta J=2$) $E2$ transitions. The dipole sequences with strong $M1$ transitions appear at excitation energies of about 2.5 MeV and coexist with the collective structures. Since these $M1$ bands display also fairly strong stretched $E2$ transitions, there is an obvious difference to the shears bands occurring on top of an irregular level scheme as, e.g., in ^{200}Pb .

To investigate whether such $M1$ sequences can be classified as magnetic rotation and how the deformation influences their properties, we have revisited the nucleus ^{79}Br . Our present study focuses mainly on the dipole band that starts at 2.3 MeV and depopulates into the low-lying collective $E2$ bands of both positive and negative parity. Excited states in this nucleus were previously studied via $^{77}\text{Se}(\alpha, pn)$ and

*Deceased.

†Present address: Ludwig Maximilian Universität München, D-85748 Garching, Germany.

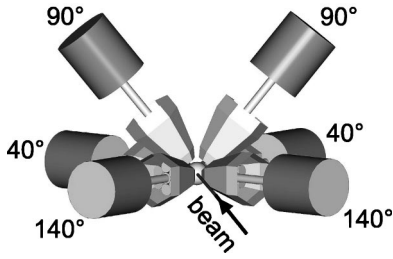


FIG. 1. Arrangement of the six CLUSTER detectors used in the present experiment.

II. EXPERIMENTAL METHODS AND RESULTS

Excited states in ^{79}Br were populated using the $^{76}\text{Ge}(^7\text{Li},4n)$ reaction at a beam energy of 35 MeV. The beam was delivered by the MP tandem accelerator of the Max-Planck-Institut für Kernphysik Heidelberg. Emitted γ rays were measured with six EUROBALL CLUSTER detectors [34] positioned at $\pm 40^\circ, \pm 90^\circ$, and $\pm 140^\circ$ relative to the beam direction. While the four detectors at $\pm 40^\circ$ and $\pm 140^\circ$ were placed in a horizontal plane, the two detectors at $\pm 90^\circ$ were tilted out of this plane by 52° to achieve a distance of 25 cm between the target and each of the 42 HPGe crystals. This detector arrangement is illustrated in Fig. 1. Special lead collimators were mounted in front of the CLUSTER detectors to prevent the escape-suppression shields from being hit directly by the γ rays. Two experiments were performed: one with a thin target consisting of 0.2 mg cm^{-2} ^{76}Ge on a 0.05 mg cm^{-2} carbon backing, and one with a thick target of 0.6 mg cm^{-2} ^{76}Ge evaporated onto a 2.5 mg cm^{-2} gold backing. The thickness of the gold backing was chosen such that the recoil nuclei are completely stopped in the backing, thus enabling the determination of mean level lifetimes using the Doppler-shift-attenuation (DSA) method. In each of these experiments about 7×10^8 coincidence events of fold 2 or higher were measured. The γ - γ coincidence events were sorted off-line into E_γ - E_γ matrices for either all or specific detector combinations. In addition, an E_γ - E_γ - E_γ cube of γ - γ - γ events was created. Coincidence spectra were extracted from the matri-

$^{78}\text{Se}(\alpha,p2n)$ reactions [27]. In that work a sequence of four $M1$ transitions built on a $13/2^-$ state at 2.4 MeV was observed. Transition strengths of $B(M1) \approx 0.3\text{--}0.6$ W.u. were derived for three transitions. During our present investigation we became aware of a study of ^{79}Br using the $^{76}\text{Ge}(^7\text{Li},4n)$ reaction [33] in which all bands were extended by about two transitions and five values or limits of level lifetimes were determined in addition to the known ones [33]. In the present work the $M1$ band was extended by four $M1$ transitions up to a $(29/2^-)$ state at 6.4 MeV. Moreover, $E2$ crossover transitions were observed within this band for the first time. The collective $E2$ bands built on the isomeric $9/2^+$ state and the $3/2^-$ ground state were established up to $(37/2^+)$ and $(37/2^-)$ states, respectively, at about 8.8 MeV. Mean lifetimes were deduced for 17 levels.

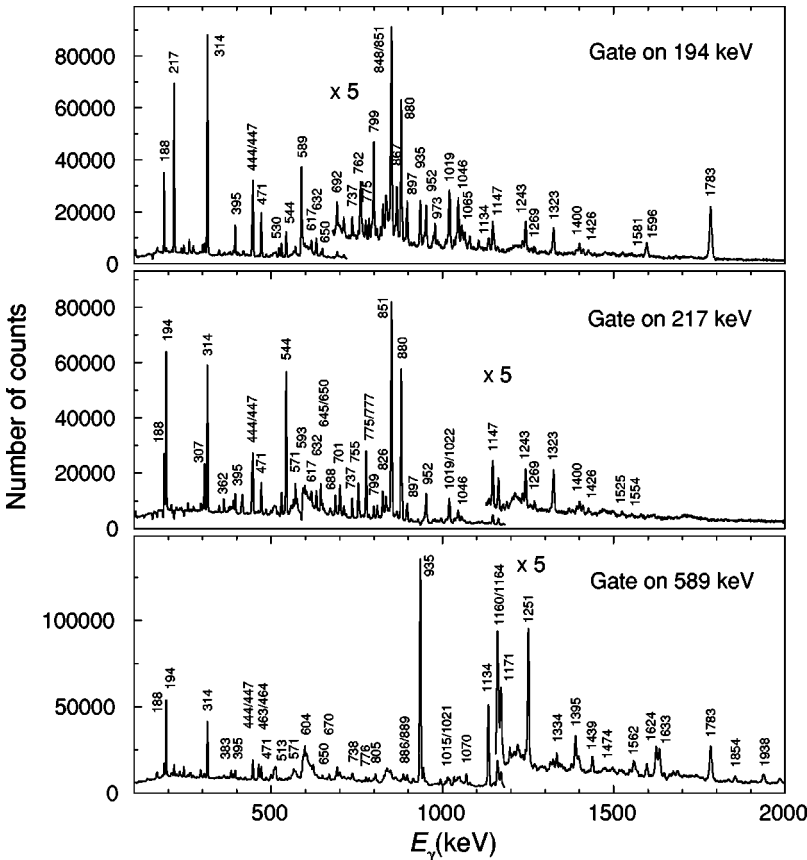


FIG. 2. Examples of background-corrected γ - γ coincidence spectra. Peaks marked with their energies are assigned to ^{79}Br .

ces and the cube using the codes ESCL8R, LEVIT8R [35], and VS [36]. Examples of background-corrected γ - γ coincidence spectra are shown in Fig. 2. The γ transitions assigned to ^{79}Br on the basis of the present experiment are compiled in Table I.

A. γ - γ directional correlations

The analysis of directional correlations of coincident γ rays emitted from oriented states (DCO) was applied to deduce the multipole order of the γ rays and thus to assign spins to the emitting states. This method is based on the formalism described in Refs. [37,38] and discussed, e.g., in Ref. [39]. The DCO ratio is defined as $R_{\text{DCO}} = W(\theta_1, \theta_2, \phi) / W(\theta_2, \theta_1, \phi)$, where the quantity $W(\theta_1, \theta_2, \phi)$ denotes the coincidence intensity of a transition γ_2 measured in a detector at the angle θ_2 relative to the beam, gated with a transition γ_1 measured in a detector at the angle θ_1 . The quantity ϕ is the angle between the two planes opened by the respective target-detector axis and the beam axis. The intensity $W(\theta_2, \theta_1, \phi)$ describes the reverse case arising from an exchange of the observation angles or of the gating and observed transition. A ratio of $R_{\text{DCO}} = 1$ is obtained if the transitions γ_1 and γ_2 are stretched transitions of pure and equal multipole order. Experimental intensities W can be extracted from E_{γ_1} - E_{γ_2} coincidence matrices of selected detector pairs. Using the symmetry relation $W(\theta_1, \theta_2, \phi) = W(180^\circ - \theta_1, 180^\circ - \theta_2, \phi)$ [40] the present detector setup contained eight CLUSTER-detector pairs corresponding to $\theta_1 = 90^\circ$, $\theta_2 = 40^\circ$, $\phi = 52^\circ$. γ - γ events of these pairs were sorted into a $(90^\circ, 40^\circ)$ matrix. To keep the opening angles of the detectors small, only the three crystals of the middle vertical row of each CLUSTER detector were included. These crystals are indicated as gray areas in the front view of the CLUSTER detector shown in Fig. 3. Coincidence spectra were extracted by setting gates on certain peak and background intervals in the $(90^\circ, 40^\circ)$ and the transposed $(40^\circ, 90^\circ)$ matrices. The DCO ratios obtained for transitions in ^{79}Br are listed in Table I.

B. Linear polarization of γ rays

A CLUSTER detector represents a nonorthogonal Compton polarimeter with scattering planes at $30^\circ/150^\circ$ and 90° to the beam axis as is shown in Fig. 3. Despite this nonoptimum geometry the CLUSTER detector has a polarization efficiency comparable with orthogonal polarimeters [41]. To deduce experimental asymmetries $A = (I_{90} - aI_{30/150}) / (I_{90} + aI_{30/150})$ from intensities I of γ rays Compton scattered within the 90° and $30^\circ/150^\circ$ planes, γ - γ events of two neighboring crystals in the CLUSTER detectors at 90° to the beam were restored and sorted into respective spectra, whereas coincidence events including signals of more than two crystals (multiple Compton scattering) were rejected. The normalization factor was determined to $a = 0.49(2)$ from intensities of γ transitions of a ^{152}Eu calibration source that are isotropic ($A = 0$). This normalization factor is close to the value of 0.5 resulting from the numbers of detector pairs in the 90° plane (four pairs) and the $30^\circ/150^\circ$ plane

(eight pairs) and reflects almost identical efficiencies of all detectors. The asymmetries deduced from this analysis are given in Table I and have been used to determine the multiplicities of the γ rays.

C. Level lifetimes

Mean lifetimes were determined from Doppler shifts of γ rays observed in coincidence spectra at angles of 40° and 140° to the beam direction using the DSA method. These coincidence spectra were extracted from two E_{γ_1} - E_{γ_2} matrices containing coincidence events of all Ge detector pairs that include one detector of the middle vertical rows (cf. Fig. 3) of the CLUSTER detectors at 40° or 140° , respectively. The spectra were obtained from gating on transitions below the considered ones because of the much better statistics in this case. The lifetimes were deduced from a comparison of experimental with calculated line shapes. The velocity distributions of the emitting nuclei were calculated with a Monte Carlo code taking into account reactions at different depths in the target, the kinematics of the reaction and the slowing down and deflection of the recoils [42]. For the slowing down the cross sections given in Ref. [43] were used with correction factors of $f_e = 0.9$ and $f_n = 0.7$ for the electronic and nuclear stopping powers, respectively [44]. The sidefeeding time was assumed to be zero for an excitation energy of 9 MeV. This energy represents roughly the maximum excitation energy of the final nucleus $E^* = E_{7\text{Li}}^{\text{CM}} + Q - 4 \cdot E_n$ with a value of $Q = -14.5$ MeV and a mean energy of the emitted neutrons of $E_n \approx 2$ MeV. With decreasing excitation energy an increase of the sidefeeding time according to $\tau_{\text{sf}} = (9 - E/\text{MeV}) \cdot 0.03$ ps was assumed, which had been proven to be a good approach [44]. Examples of the line-shape analysis are shown in Fig. 4. The lifetimes obtained from this analysis as well as from previous work [27,33] are given in Table II. The errors of these lifetimes include statistical errors, uncertainties of lifetimes of the feeding levels, and uncertainties of the intensities of the feeding transitions and the sidefeeding. The influence of variations of the small sidefeeding times on the level lifetimes is small compared with the influence of the bigger lifetimes of the feeding levels or with the influence due to the uncertainties of the intensities of feeding transitions.

The values deduced from the present analysis are generally smaller than those from the previous studies. However, they agree within the errors except the lifetimes of the states at 1957, 3535, and 5506 keV. The reason for the difference may be (i) the cascade feeding from higher lying states that could not be taken into account in previous work because these states and their lifetimes were not known, (ii) the different parametrizations of the sidefeeding time. The parametrization used in Ref. [33] neglects sidefeeding for excitation energies greater than 4.4 MeV, which is 5 MeV below the highest states found in the present study. Transition strengths deduced from the present lifetimes are listed in Table III.

III. LEVEL SCHEME

The level scheme of ^{79}Br deduced from the present experiment is shown in Fig. 5. It results from the analysis of

TABLE I. γ transitions assigned to ^{79}Br .

E_γ^a (keV)	I_γ^b	R_{DCO}^c	E_{GATE}^d (keV)	A^e	$\sigma\lambda^f$	$J_i^{\pi g}$	$J_f^{\pi h}$	E_i^i (keV)
104.3	0.5(1)	0.9(2)	194		$M1$	$15/2^-$	$13/2^-$	2580
187.6	3.2(3)	1.02(9)	314		$M1$	$15/2^-$	$13/2^-$	2580
193.8	11(1)	0.55(3)	589		$M1$	$17/2^-$	$15/2^-$	2774
207.5 ^j					$E3$	$9/2^+$	$3/2^-$	208
217.1	36(4)					$5/2^-$	$3/2^-$	217
234.9	0.4(1)					$13/2^-$	$11/2^-$	1948
238.0	1.1(1)					$7/2^-$		762
256.9	1.0(1)					$17/2^-$	$15/2^-$	2725
261.1	2.9(4)	0.9(2)	194		$M1$	$5/2^{(-)}$	$3/2^-$	261
300.7	0.6(1)	1.0(2)	194		$M1$	$15/2^-$		2580
304.9	1.6(2)	1.0(1)	314		$M1$	$17/2^-$	$15/2^-$	2774
306.6	1.9(2)	0.65(8)	880		$M1$	$9/2^-$	$7/2^-$	1068
314.0	11(1)	0.50(3)	589		$M1$	$19/2^-$	$17/2^-$	3088
348.6	0.6(1)						$21/2^-$	3908
362.2	0.7(1)	0.6(1)	851		$M1$	$19/2^-$	$17/2^-$	3088
380.6	0.9(1)					$11/2^-$		1714
383.2	0.9(1)			-0.02(1)	$(M1)$	$11/2^+$	$13/2^+$	1181
389.9	1.3(1)	0.5(1)	701		$M1$	$21/2^-$	$19/2^-$	3560
395.0	2.1(2)	0.49(8)	851		$M1$	$19/2^-$	$17/2^-$	3170
442.8	0.2(1)					$19/2^-$	$17/2^-$	3170
444.2	1.9(2)	0.8(1) ^k	851		$(M1)$	$13/2^-$	$13/2^-$	2393
446.7	4.6(5)	0.49(7) ^l	851	-0.03(1)	$M1$	$21/2^-$	$19/2^-$	3535
447.6	1.3(1)				$(M1)$	$11/2^{(-)}$		1781
462.6	0.5(1)					$21/2^+$	$19/2^+$	3366
464.0	1.4(1)	0.46(6)	589		$M1$	$17/2^+$	$15/2^+$	2421
471.2	3.1(3)	0.46(7)	589		$M1$	$21/2^-$	$19/2^-$	3560
501.7	3.2(3)			-0.10(3)	$(M1)$	$13/2^+$	$11/2^+$	1683
508.1	1.3(1)					$23/2^-$	$21/2^-$	4067
512.9	0.4(1)					$(29/2^+)$	$29/2^+$	6020
513.6	1.6(2)					$25/2^-$	$23/2^-$	4581
521.9	0.5(1)	0.5(2)	700		$M1$	$15/2^-$	$13/2^-$	2469
523.3	2.7(5)						$3/2^-$	523
530.3	1.5(2)	1.0(2)	880		$(M1)$	$13/2^-$	$13/2^-$	2477
543.9	7.7(8)	0.7(1)	701	-0.10(1)	$M1$	$7/2^-$	$5/2^-$	762
565.3	1.8(2)						$11/2^-$	2280
570.6	1.1(1)					$23/2^+$	$21/2^+$	3936
571.2	3.5(4)	0.9(2)	762				$7/2^-$	1333
589.0	100(2)			0.08(1)	$E2$	$13/2^+$	$9/2^+$	797
593.5	3.8(4)					$23/2^-$	$21/2^-$	4153
603.9	1.8(2)					$(25/2^+)$	$25/2^+$	4721
611.6	1.8(2)	0.5(1)	851		$M1$	$13/2^-$	$11/2^{(-)}$	2393
617.4	3.0(3)	0.5(1)	851	-0.01(1)	$M1$	$23/2^-$	$21/2^-$	4153
631.7	1.9(2)	0.49(8)	880		$M1$	$15/2^-$	$13/2^-$	2580
644.9	2.4(2)	0.57(7)	851	-0.08(2)	$M1$	$11/2^-$	$9/2^-$	1714
649.9	1.5(2)	0.4(1)	851	-0.06(3)	$M1$	$25/2^-$	$23/2^-$	4803
669.6	0.9(1)						$21/2^{(+)}$	4341
687.7	3.6(4)					$15/2^-$	$11/2^{(-)}$	2469
692.5	2.1(2)					$(7/2^-)$	$5/2^{(-)}$	954
700.7	5.1(5)	0.9(2)	851	0.07(1)	$E2$	$19/2^-$	$15/2^-$	3170
712.3	1.2(1)					$11/2^{(-)}$	$9/2^-$	1781
736.7	1.4(1)	0.5(1)	701		$(E1)$	$15/2^-$	$17/2^+$	2469
737.1	1.5(2)					$(7/2^-)$	$5/2^-$	954

TABLE I. (*Continued.*)

E_γ^a (keV)	I_γ^b	R_{DCO}^c	E_{GATE}^d (keV)	A^e	$\sigma\lambda^f$	$J_i^{\pi g}$	$J_f^{\pi h}$	E_i^i (keV)
738.5	3.7(4)	1.0(1)	589	0.05(1)	$E2$	$17/2^+$	$13/2^+$	2421
754.9	4.8(5)	0.9(1)	701	0.07(2)	$E2$	$15/2^-$	$11/2^-$	2469
759.4	1.4(1)					$11/2^-$	$(7/2^-)$	1714
760.3	0.8(1)					$21/2^-$	$17/2^-$	3535
761.5	4.4(4)	0.9(3)	880	0.01(1)	$(E2)$	$7/2^-$	$3/2^-$	762
769.3	0.4(1)					$21/2^{(+)}$	$19/2^+$	3671
775.4	0.7(1)	1.0(4)	194		$M1$	$27/2^-$	$25/2^-$	5579
776.5	0.8(1)	1.1(4)	589	0.03(1)	$E2$	$15/2^+$	$11/2^+$	1957
777.4	5.9(6)	0.87(6)	851	0.03(1)	$(E2)$	$17/2^-$	$13/2^-$	2725
785.3	1.0(1)					$(25/2^+)$	$23/2^+$	4721
785.8	1.0(1)					$21/2^-$	$17/2^-$	3560
799.4	2.4(2)	1.5(1)	194		$E2$	$15/2^-$	$11/2^{(-)}$	2580
804.7	1.8(2)					$21/2^{(+)}$	$21/2^+$	3671
805.4	0.4(1)					$(29/2^-)$	$27/2^-$	6384
809.2	1.0(1)							1333
809.9	1.6(2)	1.0(2) ^m	880		$E2$	$21/2^-$	$17/2^-$	3535
820.5	0.5(1)						$19/2^-$	3908
825.7	2.1(2)	1.0(2)	880		$E2$	$17/2^-$	$13/2^-$	2774
827.0	2.5(3)					$11/2^{(-)}$	$(7/2^-)$	1781
834.6	2.5(2)	0.9(2)	777		$(E2)$	$21/2^-$	$17/2^-$	3560
847.5	2.3(2)					$15/2^-$	$17/2^+$	2580
851.3	19(2)			0.05(1)	$(E2)$	$9/2^-$	$5/2^-$	1068
866.7	1.6(2)	1.5(3)	194		$E2$	$15/2^-$	$11/2^-$	2580
880.0	15(2)	0.91(4)	851	0.07(1)	$E2$	$13/2^-$	$9/2^-$	1948
885.8	1.8(2)	1.0(2)	589		$(M1)$	$13/2^+$	$13/2^+$	1683
888.7	0.7(1)					$(29/2^+)$	$27/2^+$	6020
897.0	4.3(4)	0.9(1)	701	0.06(1)	$E2$	$23/2^-$	$19/2^-$	4067
914.4	1.1(1)						$19/2^+$	3817
935.2	51(5)	1.00(2)	589	0.07(1)	$E2$	$17/2^+$	$13/2^+$	1732
944.3	3.6(4)	0.9(1) ⁿ	589	0.11(1) ⁿ	$(E2)$	$21/2^+$	$17/2^+$	3366
945.4	1.9(2)	0.9(1) ⁿ	589	0.11(1) ⁿ	$(E2)$	$19/2^+$	$15/2^+$	2903
947.4	1.9(2)							2280
950.8	0.9(1)						$21/2^+$	3817
952.3	4.8(5)	1.1(2)	701	0.06(1)	$E2$	$11/2^-$	$7/2^-$	1714
953.9	1.0(1)					$(7/2^-)$	$3/2^-$	954
955.8	1.1(1)							3236
973.2	7(1)	0.7(2)	776	0.04(1)	$(M1)$	$11/2^+$	$9/2^+$	1181
977.9	0.8(1)					$23/2^-$	$19/2^-$	4067
1015.4	1.7(2)	0.4(1)	1251		$M1$	$27/2^+$	$25/2^+$	5132
1019.3	2.8(3)	1.1(2)	762		$E2$	$11/2^{(-)}$	$7/2^-$	1781
1021.0	0.6(1)					$31/2^+$	$29/2^+$	6527
1021.8	2.5(3)	1.0(3)	851	0.08(1)	$E2$	$25/2^-$	$21/2^-$	4581
1034.1	2.1(2)			0.02(1)	$(E2)$	$23/2^+$	$19/2^+$	3936
1046.2	2.7(3)	1.0(2)	851		$E2$	$25/2^-$	$21/2^-$	4581
1050.0	0.9(1)					$(25/2^+)$	$21/2^{(+)}$	4721
1056.7	1.3(1)	1.6(5)	314		$(E2)$			4965
1064.9	0.7(1)	1.7(4)	194		$E2$	$23/2^-$	$19/2^-$	4153
1069.9	3.3(3)	0.36(4)	589	0.04(3)	$M1/E2$	$23/2^+$	$21/2^+$	3936
1079.2	0.9(1)	1.0(4)	935		$E2$			4897
1082.8	0.2(1)					$(35/2^+)$	$(33/2^+)$	8150
1115.5	0.3(1)						$5/2^-$	1333
1134.2	24(2)	1.02(3)	589	0.07(1)	$E2$	$21/2^+$	$17/2^+$	2867

TABLE I. (*Continued.*)

E_γ^a (keV)	I_γ^b	R_{DCO}^c	E_{GATE}^d (keV)	A^e	$\sigma\lambda^f$	$J_i^{\pi g}$	$J_f^{\pi h}$	E_i^i (keV)
1134.6	1.0(1)						17/2 ⁻	3908
1147.4	2.7(3)	0.8(2)	701		<i>E2</i>	27/2 ⁻	23/2 ⁻	5214
1160.4	7.7(8)	0.50(3)	589		<i>M1</i>	15/2 ⁺	13/2 ⁺	1957
1164.4	3.4(3)	0.9(2)	935	0.08(3)	<i>E2</i>	25/2 ⁺	21/2 ⁺	4530
1170.9	4.9(5)	0.42(4)	935	-0.01(1)	<i>M1/E2</i>	19/2 ⁺	17/2 ⁺	2903
1196.3	1.5(2)					27/2 ⁺	23/2 ⁺	5132
1234.3	0.6(1)							6199
1242.8	2.1(2)	1.5(2)	194		<i>E2</i>	29/2 ⁻	25/2 ⁻	5824
1250.7	9.0(9)	0.97(5)	589	0.09(1)	<i>E2</i>	25/2 ⁺	21/2 ⁺	4118
1268.6	0.4(1)					25/2 ⁻	21/2 ⁻	4803
1298.3	0.4(1)					(29/2 ⁺)	(25/2 ⁺)	6020
1322.8	1.1(1)	1.0(3)	701		<i>E2</i>	31/2 ⁻	27/2 ⁻	6537
1325.1	1.2(1)	1.1(2)	851	0.02(2)	<i>E2</i>	13/2 ⁻	9/2 ⁻	2393
1333.6	1.4(1)	0.9(3)	589		(<i>E2</i>)	(29/2 ⁺)	25/2 ⁺	5864
1388.2	2.6(3)	0.9(1)	1251	0.07(2)	<i>E2</i>	29/2 ⁺	25/2 ⁺	5506
1392.4	0.3(1)							7592
1395.0	0.7(1)	1.0(2)	589		<i>E2</i>	31/2 ⁺	27/2 ⁺	6527
1400.2	0.9(1)					(33/2 ⁻)	29/2 ⁻	7224
1410.2	0.4(1)					13/2 ⁻	9/2 ⁻	2477
1426.5	0.5(1)					27/2 ⁻	23/2 ⁻	5579
1437.6	1.3(1)					19/2 ⁻	17/2 ⁺	3170
1439.3	0.6(1)						19/2 ⁺	4341
1474.2	0.6(1)						21/2 ⁺	4341
1475.3	2.0(2)			0.04(2)	(<i>E2</i>)	13/2 ⁺	9/2 ⁺	1683
1516.1	0.4(1)					(33/2 ⁺)	(29/2 ⁺)	7380
1524.8	0.3(1)					(35/2 ⁻)	31/2 ⁻	8062
1553.5	0.2(1)					(37/2 ⁻)	(33/2 ⁻)	8777
1561.6	0.7(1)	0.8(2)	1134		(<i>E2</i>)	(33/2 ⁺)	29/2 ⁺	7068
1580.9	0.3(1)					(29/2 ⁻)	25/2 ⁻	6384
1596.3	1.5(2)	1.2(3)	589		(<i>E1</i>)	13/2 ⁻	13/2 ⁺	2393
1622.2	0.3(1)					(35/2 ⁺)	31/2 ⁺	8150
1624.4	2.8(3)	0.9(1)	589	0.07(2)	<i>E2</i>	17/2 ⁺	13/2 ⁺	2421
1633.4	2.8(3)	1.0(1)	589	0.06(2)	<i>E2</i>	21/2 ⁺	17/2 ⁺	3366
1664.2	0.7(1)	1.3(5)	1134	0.17(8)	<i>E2</i>	25/2 ⁺	21/2 ⁺	4530
1744.6	0.2(1)					(37/2 ⁺)	(33/2 ⁺)	8812
1783.1	3.5(4)	0.57(5)	589	0.04(1)	<i>E1</i>	15/2 ⁻	13/2 ⁺	2580
1854.5	0.7(1)					(25/2 ⁺)	21/2 ⁺	4721
1902.1	0.3(1)					(29/2 ⁺)	25/2 ⁺	6020
1937.5	1.1(1)	1.1(3)	935		(<i>E2</i>)	21/2 ⁽⁺⁾	17/2 ⁺	3671

^aTransition energy. The error is in the range of 0.1–0.5 keV.

^bRelative intensity of the γ ray normalized to $I_\gamma = 100$ of the $13/2_1^+ \rightarrow 9/2_1^+$ transition at 589.0 keV. This value was deduced from coincidence spectra.

^cDCO ratio $R_{\text{DCO}} = W(90^\circ, 40^\circ, 52^\circ) / W(40^\circ, 90^\circ, 52^\circ)$.

^dEnergy of the gating transition used for the determination of the DCO ratio.

^eAsymmetry $A = (I_{90} - aI_{30/150}) / (I_{90} + aI_{30/150})$ (see Sec. II B).

^fMultipolarity compatible with the DCO ratio.

^gSpin and parity of the initial state.

^hSpin and parity of the final state.

ⁱEnergy of the initial state.

^jThis transition deexciting the isomeric state at 207.5 keV ($\tau = 7.0$ s) was not observed in the present coincidence experiment.

^kInfluenced by the 446.7–447.6 keV doublet.

^lCombined value derived for the 446.7–447.6 keV doublet.

^mCombined value derived for the 809.2–809.9 keV doublet.

ⁿCombined value derived for the 944.3–945.4 keV doublet.

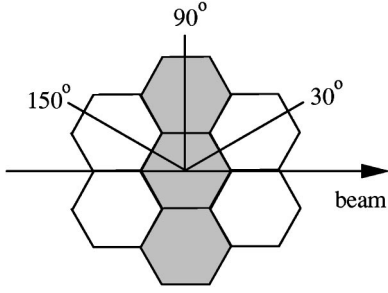


FIG. 3. Schematic front view of the seven HPGe crystals of a CLUSTER detector. The three crystals of the middle vertical row in each CLUSTER detector (marked grey) were used for analysing DCO ratios and Doppler shifts of γ rays. All crystal pairs compatible with the given scattering angles in the CLUSTER detectors at 90° to the beam were used for analyzing the linear polarization of γ rays.

γ - γ coincidence relations and γ -ray intensities. The spin and parity assignments are based on DCO ratios and polarization data of the γ rays and are supported by deexcitation modes and level lifetimes. Extensions of the level scheme with respect to previous work are discussed in the following.

The positive-parity yrast band built on the $9/2^+$ isomeric state with $T_{1/2}=4.9$ s (band A in Fig. 5) has been known up to $(33/2^+)$ and $(23/2^+)$ states for the signatures $\alpha = +1/2$ and $\alpha = -1/2$ ($\alpha = J \bmod 2$), respectively, in Ref. [33]. In the present work it has been extended up to states with J^π

TABLE II. Mean lifetimes of states in ^{79}Br .

E_i (keV) ^a	E_γ (keV) ^b	τ (ps)		
		This work ^c	Ref. [27]	Ref. [33]
1732	935.2	1.1(3)	1.7(3)	
1957	1160.4	0.3(1)		0.75(25)
2725	777.4	0.8(4)		
2867	1134.2	0.40(6)	0.6(2)	0.63(25)
2903	1170.9	0.25(7)		
3088	314.0	1.1(3)	$1.4^{+0.7}_{-0.6}$	
3535	809.9	0.55(15)	1.1(2)	1.0(3)
3560	471.2	0.6(2)		
3936	1069.9	0.27(5)		≤ 1
4118	1250.7	0.23(3)	0.4(2)	$0.36^{+0.25}_{-0.15}$
4153	617.4	0.20(4)		≤ 0.5
4530	1164.4	0.5(1) ^d		
4581	1046.2	0.37(8)		
4803	649.9	0.17(3)		
5506	1388.2	0.07(3)		0.42(15)
5824	1242.8	0.14(4)		
6527	1395.0	0.24(8)		

^aLevel energy.

^bEnergy of the γ transition used for the line-shape analysis in connection with the DSA method.

^cMean lifetime. The error in parentheses includes the statistical error, uncertainties of feeding times and feeding intensities, and a 10% uncertainty of the nuclear and electronic stopping power.

^dEffective lifetime without feeding correction.

$= (37/2^+)$ and $J^\pi = (35/2^+)$, respectively. In the second $\alpha = +1/2$ band (band B in Fig. 5), $(29/2^+)$ and $(33/2^+)$ states have been identified in addition to previous work [33]. Besides, a new sequence of probably $(21/2^+)$, $(25/2^+)$, and $(29/2^+)$ states and several interband transitions have been found.

The $\alpha = +1/2$ sequence of the negative-parity band built on the $3/2^-$ ground state (band C in Fig. 5) has been extended by three transitions up to the $(37/2^-)$ state. The 994 keV transition tentatively proposed on top of the $23/2^-$ state in Ref. [33] could not be confirmed in our experiment. Instead we have observed a 1147 keV transition and two further transitions on top which extended the $\alpha = -1/2$ branch

TABLE III. Experimental transition strengths in ^{79}Br .

E_i (keV)	E_γ (keV)	J_i^π	J_f^π	$\sigma\lambda$	$B(\sigma\lambda)^a$ (W.u.)
1732	935.2	$17/2^+$	$13/2^+$	$E2$	52^{+19}_{-11}
2867	1134.2	$21/2^+$	$17/2^+$	$E2$	54^{+10}_{-7}
4118	1250.7	$25/2^+$	$21/2^+$	$E2$	58^{+9}_{-7}
5506	1388.2	$29/2^+$	$25/2^+$	$E2$	112^{+84}_{-34}
1957	1160.4	$15/2^+$	$13/2^+$	$M1$	$0.07^{+0.04}_{-0.02}$
	776.5	$15/2^+$	$11/2^+$	$E2$	48^{+44}_{-20}
2903	1170.9	$19/2^+$	$17/2^+$	$M1$	$0.06^{+0.03}_{-0.02}$
	945.4	$19/2^+$	$15/2^+$	$E2$	60^{+36}_{-20}
3936	570.6	$23/2^+$	$21/2^+$	$M1$	$0.11^{+0.05}_{-0.03}$
	1069.9	$23/2^+$	$21/2^+$	$M1$	$0.05^{+0.02}_{-0.01}$
	1034.1	$23/2^+$	$19/2^+$	$E2$	41^{+16}_{-11}
6527	1021.0	$31/2^+$	$29/2^+$	$M1$	$0.06^{+0.04}_{-0.02}$
	1395.0	$31/2^+$	$27/2^+$	$E2$	17^{+12}_{-7}
2726	256.9	$17/2^-$	$15/2^-$	$M1$	$0.4^{+0.5}_{-0.2}$
	777.4	$17/2^-$	$13/2^-$	$E2$	150^{+160}_{-50}
3560	389.9	$21/2^-$	$19/2^-$	$M1$	$0.14^{+0.12}_{-0.06}$
	471.2	$21/2^-$	$19/2^-$	$M1$	$0.19^{+0.15}_{-0.07}$
	834.6	$21/2^-$	$17/2^-$	$E2$	48^{+40}_{-18}
	785.8	$21/2^-$	$17/2^-$	$E2$	28^{+25}_{-11}
4581	513.6	$25/2^-$	$23/2^-$	$M1$	$0.15^{+0.07}_{-0.05}$
	1021.8	$25/2^-$	$21/2^-$	$E2$	36^{+16}_{-10}
	1046.2	$25/2^-$	$21/2^-$	$E2$	35^{+16}_{-10}
5824	1242.8	$29/2^-$	$25/2^-$	$E2$	98^{+39}_{-22}
3088	314.0	$19/2^-$	$17/2^-$	$M1$	$0.88^{+0.35}_{-0.18}$
	362.2	$19/2^-$	$17/2^-$	$M1$	$0.04^{+0.03}_{-0.02}$
3535	446.7	$21/2^-$	$19/2^-$	$M1$	$0.43^{+0.20}_{-0.13}$
	760.3	$21/2^-$	$17/2^-$	$E2$	33^{+22}_{-13}
	809.9	$21/2^-$	$17/2^-$	$E2$	48^{+30}_{-17}
4153	617.4	$23/2^-$	$21/2^-$	$M1$	$0.27^{+0.11}_{-0.08}$
	593.5	$23/2^-$	$21/2^-$	$M1$	$0.38^{+0.15}_{-0.10}$
	1064.9	$23/2^-$	$19/2^-$	$E2$	14^{+7}_{-5}
4803	649.9	$25/2^-$	$23/2^-$	$M1$	$0.53^{+0.17}_{-0.12}$
	1268.6	$25/2^-$	$21/2^-$	$E2$	15^{+9}_{-6}

^aExperimental reduced transition strengths derived from the lifetimes given in Table II and from the intensities in Table I. Weisskopf units are: $1 \text{ W.u.}(M1) = 1.79 \mu_N^2$; $1 \text{ W.u.}(E2) = 20.13 e^2 \text{fm}^4$.

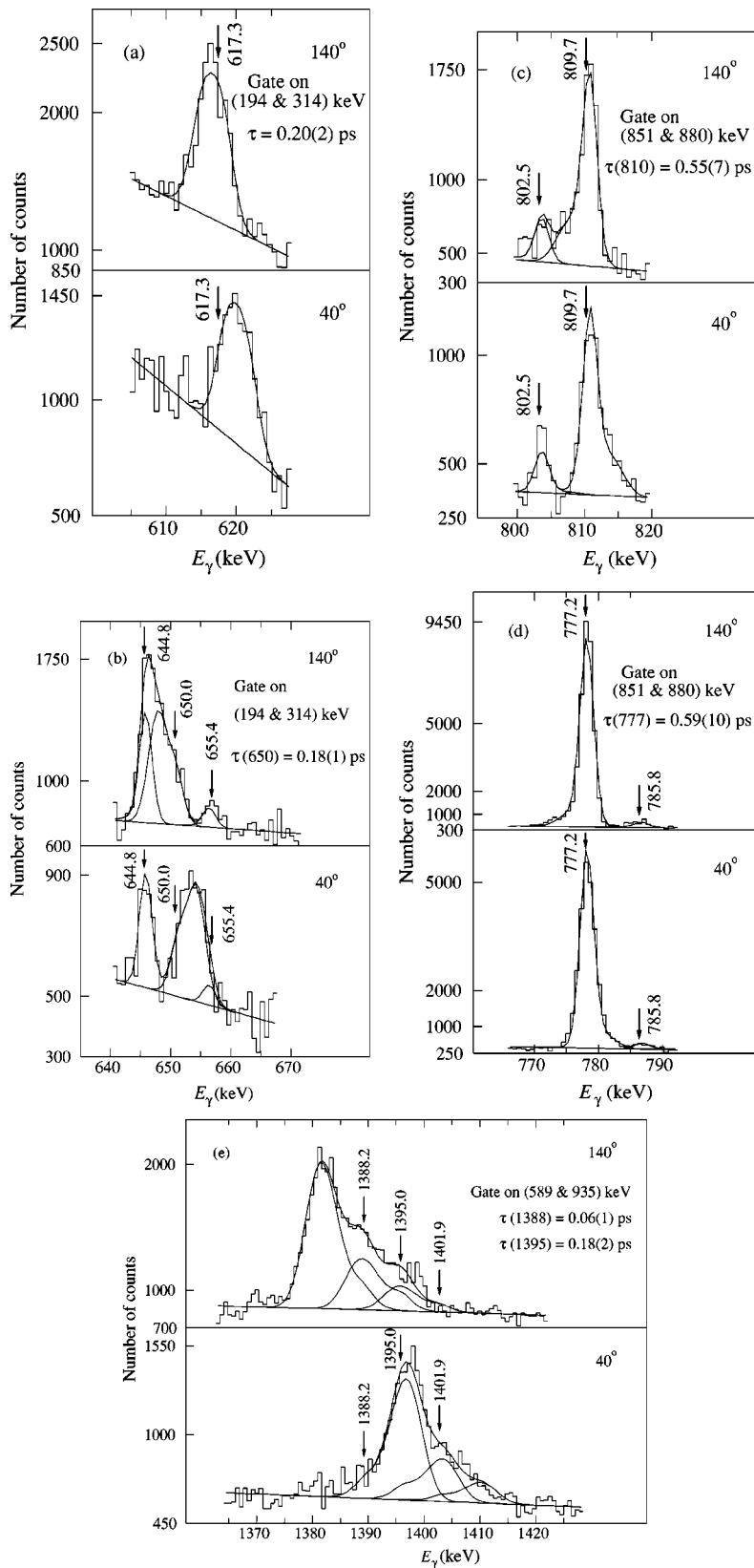


FIG. 4. Examples of the line-shape analysis using the DSA method. Lifetimes were deduced from a joint fit of calculated to experimental line shapes at the complementary observation angles of 40 and 140°. Feeding corrections are included. The values of energies, lifetimes, and their errors are results of the presented fits.

up to the $(35/2^-)$ state. In addition, seven new intraband $M1$ transitions have been found. The level sequence starting with the state at 523 keV has been extended by two states and interband transitions linking these states with states of the ground-state band.

The $\Delta J=1$ band starting with the $13/2^-$ state at 2393 keV (band D in Fig. 5) has been known up to the $23/2^-$ state [27,33]. In the present study this band could be established up to the $(29/2^-)$ state. Moreover, $\Delta J=2$ crossover transitions have been observed for the first time in this band. Fur-

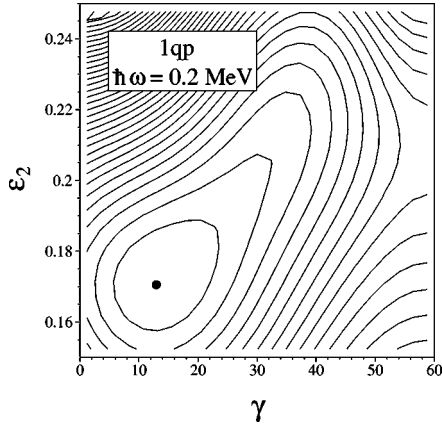


FIG. 6. Total Routhian surface for the $1qp$ configuration $\pi(g_{9/2})$ in ^{79}Br as a function of the quadrupole deformation ϵ_2 and the triaxial deformation γ at a rotational frequency of $\hbar\omega = 0.2$ MeV. The distance between the contour lines is 25 keV.

thermore, a cascade of transitions at 1057, 1234, and 1392 keV has been identified on top of a 3908 state which populates the $17/2^-$ and $19/2^-$ states of the $\Delta J = 1$ band.

IV. DISCUSSION

Three different band structures emerge from the level scheme of ^{79}Br shown in Fig. 5:

(i) the positive-parity yrast band based on the $9/2^+$ isomeric state consisting of two signature branches with $\alpha = +1/2$ and $\alpha = -1/2$ (band A in Fig. 5) and the $\alpha = +1/2$ yrare band (band B in Fig. 5),

(ii) the $3/2^-$ ground-state band with $\alpha = +1/2$ and $\alpha = -1/2$ branches (band C in Fig. 5),

(iii) The $M1$ band starting at a $13/2^-$ state (band D in Fig. 5).

The bands A, B, and C are dominated by stretched $E2$ transitions and were interpreted in Ref. [33] in terms of the principal-axis cranked-shell (PAC) model as well as the

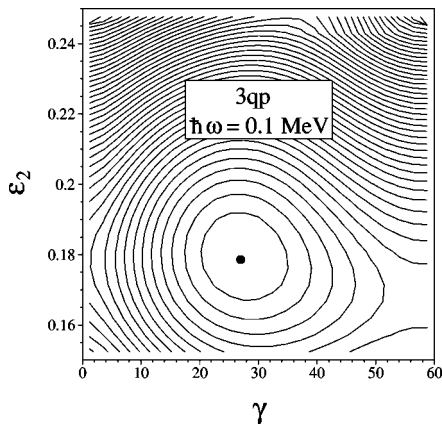


FIG. 7. Total Routhian surface for the $3qp$ configuration $\pi(g_{9/2}) \nu(g_{9/2}) \nu(fp)$ in ^{79}Br as a function of the quadrupole deformation ϵ_2 and the triaxial deformation γ at a rotational frequency of $\hbar\omega = 0.1$ MeV. The distance between the contour lines is 25 keV.

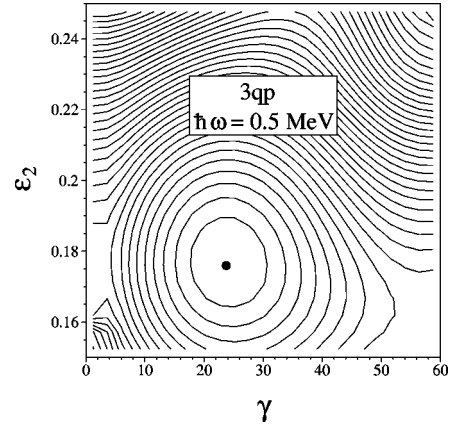


FIG. 8. Total Routhian surface for the $3qp$ configuration $\pi(g_{9/2}) \nu(g_{9/2}) \nu(fp)$ in ^{79}Br as a function of the quadrupole deformation ϵ_2 and the triaxial deformation γ at a rotational frequency of $\hbar\omega = 0.5$ MeV. The distance between the contour lines is 25 keV.

particle-rotor model (PRM). In these calculations a quadrupole deformation of $\epsilon_2 \approx 0.2$ was used which is consistent with experimental $B(E2)$ values [27]. However, a triaxial deformation was not considered.

We discuss the band structures A, B, and D with emphasis on the description of the $M1$ band. The midshell nuclide ^{79}Br is supposed to have a transitional character, i.e., its shape is expected to be soft with respect to changes of the deformation. Therefore we start with calculations of the total Routhian surfaces (TRS), which allows us to determine the shape parameters self-consistently and to take into account also possible variations of these parameters with spin and configuration. For this purpose, the hybrid version of the TAC model [45] has been applied together with the shell-correction method, which was successful for describing chiral rotation in triaxial nuclei [46]. Pairing has been taken into account by using values of $\Delta_\pi = 1.37$ MeV and $\Delta_\nu = 1.04$ MeV calculated according to Eq. (4) in Ref. [47]. In the TAC approach the equilibrium values for the deformation parameters (ϵ_2, γ) are determined from the TRS minimum in conjunction with a stable rotational axis which is in general tilted with respect to the principal deformation axes ($k = 1, 2, 3$). In the considered cases the value of the hexadecupole deformation ϵ_4 at the equilibrium turned out to be practically zero.

The resulting TRS for the one-quasiparticle ($1qp$) configuration ($\pi(g_{9/2})_{\alpha=+1/2}$) is shown as a function of the deformation parameters (ϵ_2, γ) in Fig. 6. This configuration is representative for the rotational band A on top of the $9/2^+$ isomer. The minimum, i.e., the equilibrium shape for this configuration, appears at $\epsilon \approx 0.17$, $\gamma \approx 14^\circ$. The direction of the rotation is the 1-axis ($\theta = 90^\circ$) which confirms principal axis cranking. The corresponding shape of the nucleus is indeed rather soft, since the energy for a drastical deformation change from the equilibrium to, e.g., $\epsilon_2 = 0.22$, $\gamma = 40^\circ$ amounts to only 100 keV.

In order to select the proper TAC configuration for the $M1$ band we examined the lowest-lying three-quasiparticle ($3qp$) configuration of negative parity including the un-

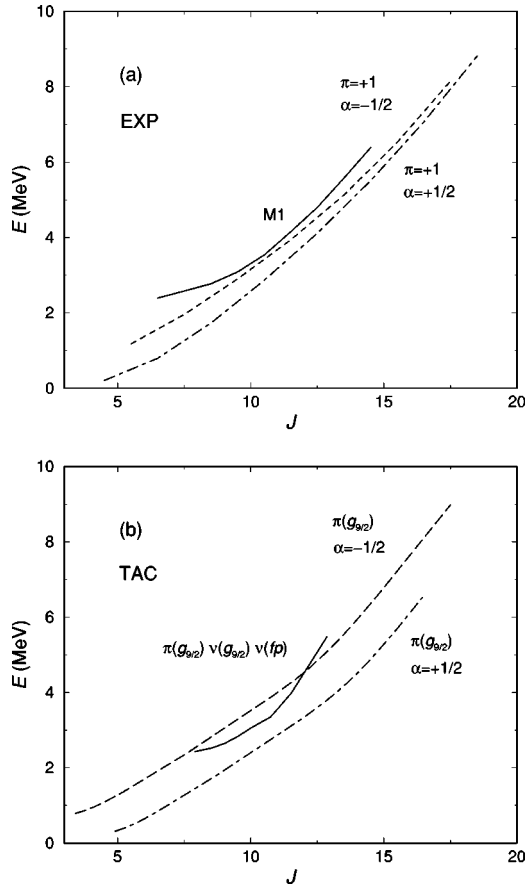


FIG. 9. (a) Experimental excitation energies as a function of the spin for the two signature branches of the positive-parity band and for the $M1$ band in ^{79}Br . (b) Calculated excitation energies as a function of the spin for the two signature branches of the $1qp$ configuration $\pi(g_{9/2})$ and for the $3qp$ configuration $\pi(g_{9/2}) \nu(g_{9/2}) \nu(fp)$ in ^{79}Br .

paired proton and a broken pair of neutrons which is $\pi(g_{9/2}) \nu(g_{9/2}) \nu(fp)$. Nearby $3qp$ configurations as $\pi(fp) \nu(g_{9/2}^2)$ and $\pi(fp) \pi(g_{9/2}^2)$ have been ruled out because they do not imply the large perpendicular components of the magnetic moment needed for strong $M1$ transitions. In Figs. 7 and 8 the TRS for the configuration $(\pi g_{9/2}) \nu(g_{9/2}) \nu(fp)$ assigned to the $M1$ band D are given for the two values $\hbar\omega = 0.1$ and 0.5 MeV, respectively.

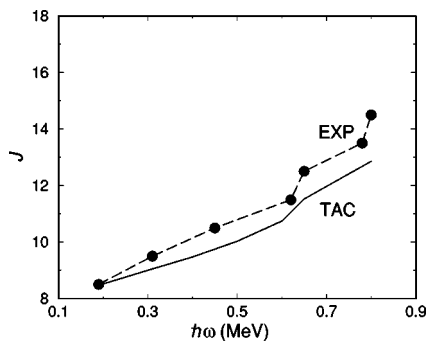


FIG. 10. Spin versus rotational frequency for the experimental and calculated $M1$ band in ^{79}Br .

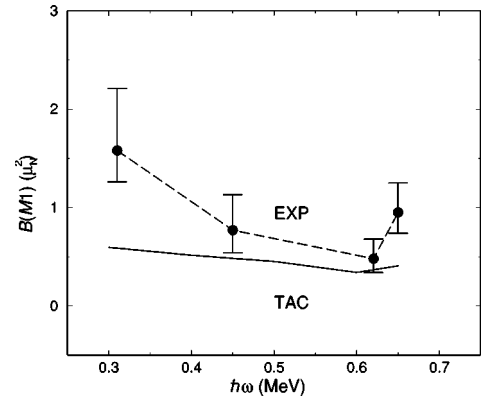


FIG. 11. Experimental and calculated $B(M1)$ values of the $M1$ band in ^{79}Br as a function of the rotational frequency.

The rotational axis is found to be tilted by an angle of $\theta \approx 60^\circ$ relative to the 3-axis within the principal plane (1,3) for the whole frequency range up to $\hbar\omega = 0.7$ MeV. The equilibrium shape is relatively stable in the ranges of $\epsilon_2 = 0.18-0.17$ and $\gamma = 27^\circ-24^\circ$ up to $\hbar\omega = 0.6$ MeV and is less soft compared with the $1q$ configuration discussed above. For $\hbar\omega > 0.6$ MeV the level density of the quasiparticle orbitals becomes high and, moreover, these levels repel each other such that a clear assignment of the quasiparticle orbitals is very complicated. Therefore an unambiguous calculation of the continuation of the $M1$ band to spins above $J \approx 13$ was not possible.

From the TRS calculations of the equilibrium shapes we obtain a quadrupole deformation of $\epsilon_2 = 0.17-0.18$ which is slightly smaller than assumed in previous calculations [33]. However, more important is the fact that triaxial deformation has to be taken into account for the $1qp$ and especially the $3qp$ band. In the excited configuration assigned to the $M1$ band, in which one neutron is lifted from an (fp) suborbital to the lowest $g_{9/2}$ orbital, the nucleus is driven to substantial triaxiality. Considering the level scheme in Fig. 5 from this point of view, the appearance of the yrare band B may be interpreted as a γ vibration on top of the $g_{9/2}$ yrast band. Furthermore, the presence of many linking transitions between all the different structures A, C, and D can be regarded

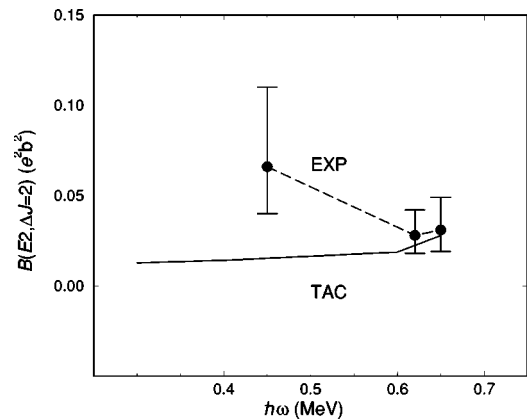


FIG. 12. Experimental and calculated $B(E2)$ values of the $M1$ band in ^{79}Br as a function of the rotational frequency.

as a typical feature of the additional mixings in a triaxially deformed system. Interestingly, it seems even possible to combine the $M1$ band D and both signature branches of the negative-parity band C to a system consisting of two connected dipole bands that resemble the chiral pairs of sister bands observed in the mass $A = 130$ region [48–51]. On the other hand, the interpretation of bands C and D in terms of chiral rotation is not directly applicable, because the calculated direction of the rotational axis corresponds to a planar tilt, whereas chiral rotation corresponds to aplanar tilts [46].

Experimental and calculated excitation energies E as a function of the spin J are presented in Fig. 9 for the $g_{9/2}$ yrast band and the $M1$ band. There is a fair agreement of the experimental data with the result of the TAC approach which confirms the configuration assignments. This conclusion is also supported by a plot of the spin J vs the rotational frequency $\hbar\omega$ for the $M1$ band given in Fig. 10. The experimental curve shows a regular behavior up to a frequency of $\hbar\omega \approx 0.6$ MeV. At higher frequency an alignment process starts in connection with a signature splitting that suggests a structural change. This behavior is well reproduced by the calculated curve. As mentioned above the avoided level crossings in the quasiparticle energies make an unambiguous calculation of the continuation of the $M1$ band to higher frequencies impossible. In Figs. 11 and 12 the $B(M1)$ and $B(E2)$ transition strengths, respectively, as calculated for the $M1$ band are compared with the experimental results. The experimental strengths are somewhat underestimated by the calculations at low frequencies. However, the TAC model provides a qualitatively reasonable description of the data. We see that the calculated $B(M1)$ strength stays almost constant at a relatively large value over the whole considered frequency range, i.e., it does not show the typical decline with increasing frequency as expected for magnetic rotation. This behavior displays that the perpendicular coupling of the two $g_{9/2}$ quasiparticles in the configuration $\pi(g_{9/2}) \nu(g_{9/2}) \nu(fp)$ cannot be realized because of the substantial triaxial deformation of $\gamma > 20^\circ$. Moreover, the

collective angular momentum does not have a definite orientation (perpendicular to the symmetry axis) as in an axially symmetric system, because its orientation can change with the spin. For the considered situation all this leads to the resulting constancy of the $B(M1)$ values as well as of the $B(E2)$ values.

V. CONCLUSIONS

In the present study the level scheme of ^{79}Br has been extended up to states with $J = (37/2)$ at $E \approx 8.8$ MeV. About 60 new transitions have been observed. Spins have been assigned to most of the about 30 new levels on the basis of the present measurement of DCO ratios. The $M1$ band has been observed up to $J^\pi = (29/2^-)$. Crossover $E2$ transitions within the $M1$ band were identified for the first time and several level lifetimes were deduced. The total Routhian surfaces calculated within the tilted-axis-cranking model predict a substantial triaxial deformation for the excited $3qp$ configuration $\pi(g_{9/2}) \nu(g_{9/2}) \nu(fp)$ assigned to the $M1$ band. The comparison of the experimental characteristics of the $M1$ band with the predictions of the TAC calculations shows that the $M1$ band can be described by this tilted configuration that implies a strong magnetic component. However, the calculated $B(M1)$ and $B(E2)$ values do not decrease with increasing rotational frequency as expected for magnetic rotation, but stay almost constant. This behavior displays the influence of the triaxial deformation and the collective angular momentum on the properties of the $M1$ band. The $M1$ band in ^{79}Br is therefore considered as a band including components of both tilted rotation causing the intense $M1$ transitions, and collective rotation of the triaxially deformed nucleus resulting in $E2$ transitions.

ACKNOWLEDGMENT

This work was supported by the Bundesministerium für Bildung, Wissenschaft, Forschung und Technologie (BMBF) under contract 06DR666I.

-
- [1] S. Frauendorf, J. Meng, and J. Reif, in Proceedings of the Conference on Physics from Large γ -Ray Detector Arrays, Berkeley, 1994, Vol. II, p. 52, LBL-35687.
 - [2] S. Frauendorf, Nucl. Phys. **A557**, 259c (1993).
 - [3] S. Frauendorf, Rev. Mod. Phys. **73**, 463 (2001).
 - [4] G. Baldsiefen, H. Hübel, W. Korten, D. Mehta, N. Nenoff, B.V. Thirumala Rao, P. Willsau, H. Grawe, J. Heese, K.H. Maier, R. Schubart, S. Frauendorf, and H.J. Maier, Nucl. Phys. **A574**, 521 (1994).
 - [5] R.M. Clark and A.O. Macchiavelli, Annu. Rev. Nucl. Part. Sci. **50**, 1 (2000).
 - [6] R.M. Clark, S.J. Asztalos, G. Baldsiefen, J.A. Becker, L. Bernstein, M.A. Deleplanque, R.M. Diamond, P. Fallon, I.M. Hibbert, H. Hübel, R. Krücken, I.Y. Lee, A.O. Macchiavelli, R.W. MacLeod, G. Schmid, F.S. Stephens, K. Vetter, R. Wadsworth, and S. Frauendorf, Phys. Rev. Lett. **78**, 1868 (1997).
 - [7] B. Fant, R.J. Tanner, P.A. Butler, A.N. James, G.D. Jones, R.J. Poynter, C.A. White, K.L. Ying, D.J.G. Love, J. Simpson, and K.A. Connell, J. Phys. G **17**, 319 (1991).
 - [8] R.M. Clark, R. Wadsworth, E.S. Paul, C.W. Beausang, I. Ali, A. Astier, D.M. Cullen, P.J. Dagnall, P. Fallon, M.J. Joyce, M. Meyer, N. Redon, P.H. Regan, W. Nazarewicz, and R. Wyss, Phys. Lett. B **275**, 247 (1992).
 - [9] G. Baldsiefen, H. Hübel, D. Mehta, B.V. Thirumala Rao, U. Birkental, G. Fröhlingdorf, M. Neffgen, N. Nenoff, S.C. Pancholi, N. Singh, W. Schmitz, K. Theine, P. Willsau, H. Grawe, J. Heese, H. Kluge, K.H. Maier, M. Schramm, R. Schubart, and H.J. Maier, Phys. Lett. B **275**, 252 (1992).
 - [10] A. Kuhnert, M.A. Stoyer, J.A. Becker, E.A. Henry, M.J. Brinkman, S.W. Yates, T.F. Wang, J.A. Cizewski, F.S. Stephens, M.A. Deleplanque, R.M. Diamond, A.O. Macchiavelli, J.E. Draper, F. Azaiez, W.H. Kelly, and W. Korten, Phys. Rev. C **46**, 133 (1992).
 - [11] R.M. Clark, R. Wadsworth, E.S. Paul, C.W. Beausang, I. Ali,

- A. Astier, D.M. Cullen, P.J. Dagnall, P. Fallon, M.J. Joyce, M. Meyer, N. Redon, P.H. Regan, J.F. Sharpey-Schafer, W. Nazarewicz, and R. Wyss, Nucl. Phys. **A562**, 121 (1993).
- [12] M. Neffgen, G. Baldsiefen, S. Frauendorf, H. Grawe, J. Heese, H. Hübel, H. Kluge, A. Korichi, W. Korten, K.H. Maier, D. Mehta, J. Meng, N. Nenoff, M. Piiparinen, M. Schönhofer, R. Schubart, U.J. van Severen, N. Singh, G. Sletten, B.V. Thirumala Rao, and P. Willsau, Nucl. Phys. **A595**, 499 (1995).
- [13] S. Frauendorf, Z. Phys. A **358**, 163 (1997).
- [14] A. Gadea, G. de Angelis, C. Fahlander, M. De Poli, E. Farnea, Y. Li, D.R. Napoli, Q. Pan, P. Spolaore, D. Bazzacco, S.M. Lenzi, S. Lunardi, C.M. Petrache, F. Brandolini, P. Pavan, C. Rossi-Alvarez, S. Sferrazza, P.G. Bizetti, A.M. Bizetti Sona, J. Nyberg, M. Lipoglavsek, J. Persson, J. Cederkäll, D. Seweryniak, A. Johnson, H. Grawe, F. Soramel, M. Ogawa, A. Makishima, R. Schubart, and S. Frauendorf, Phys. Rev. C **55**, R1 (1997).
- [15] S. Frauendorf and J. Reif, Nucl. Phys. **A621**, 736 (1997).
- [16] D.G. Jenkins, I.M. Hibbert, C.M. Parry, R. Wadsworth, D.B. Fossan, G.J. Lane, J.M. Sears, J.F. Smith, R.M. Clark, R. Krücken, I.Y. Lee, A.O. Macchiavelli, V.P. Janzen, J. Cameron, and S. Frauendorf, Phys. Lett. B **428**, 23 (1998).
- [17] D.G. Jenkins, R. Wadsworth, J. Cameron, R.M. Clark, D.B. Fossan, I.M. Hibbert, V.P. Janzen, R. Krücken, G.J. Lane, I.Y. Lee, A.O. Macchiavelli, C.M. Parry, J.M. Sears, J.F. Smith, and S. Frauendorf, Phys. Rev. C **58**, 2703 (1998).
- [18] R.M. Clark, S.J. Asztalos, B. Busse, C.J. Chiara, M. Cromaz, M.A. Deleplanque, R.M. Diamond, P. Fallon, D.B. Fossan, D.G. Jenkins, S. Juutinen, N. Kelsall, R. Krücken, G.J. Lane, I.Y. Lee, A.O. Macchiavelli, R.W. McLeod, G. Schmid, J.M. Sears, J.F. Smith, F.S. Stephens, K. Vetter, R. Wadsworth, and S. Frauendorf, Phys. Rev. Lett. **82**, 3220 (1999).
- [19] F. Brandolini, M. Ionescu-Bujor, N.H. Medina, R.V. Ribas, D. Bazzacco, M. De Poli, P. Pavan, C. Rossi-Alvarez, G. de Angelis, S. Lunardi, D. De Acuña, D.R. Napoli, and S. Frauendorf, Phys. Lett. B **388**, 468 (1996).
- [20] H. Schnare, R. Schwengner, S. Frauendorf, F. Dönau, L. Käubler, H. Prade, A. Jungclaus, K.P. Lieb, C. Lingk, S. Skoda, J. Eberth, G. de Angelis, A. Gadea, E. Farnea, D.R. Napoli, C.A. Ur, and G. Lo Bianco, Phys. Rev. Lett. **82**, 4408 (1999).
- [21] R. Schwengner, H. Schnare, S. Frauendorf, F. Dönau, L. Käubler, H. Prade, E. Grosse, A. Jungclaus, K.P. Lieb, C. Lingk, S. Skoda, J. Eberth, G. de Angelis, A. Gadea, E. Farnea, D.R. Napoli, C.A. Ur, and G. Lo Bianco, J. Res. Natl. Inst. Stand. Technol. **105**, 133 (2000).
- [22] L. Funke, F. Dönau, J. Döring, P. Kemnitz, E. Will, G. Winter, L. Hildingsson, A. Johnson, and Th. Lindblad, Phys. Lett. **120B**, 301 (1983).
- [23] R. Schwengner, J. Döring, L. Funke, G. Winter, A. Johnson, and W. Nazarewicz, Nucl. Phys. **A509**, 550 (1990).
- [24] P. Kemnitz, J. Döring, L. Funke, G. Winter, L.H. Hildingsson, D. Jerrestam, A. Johnson, and Th. Lindblad, Nucl. Phys. **A456**, 89 (1986).
- [25] J. Döring, L. Funke, G. Winter, F. Lidén, B. Cederwall, A. Johnson, R. Wyss, J. Nyberg, and G. Sletten, in *Proceedings of the International Conference on High Spin Physics and Gamma-soft Nuclei, Pittsburgh, 1990*, edited by J.X. Saladin, R.A. Sorensen, and C.M. Vincent (World Scientific, Singapore, 1991), p. 381.
- [26] J. Döring, L. Funke, R. Schwengner, and G. Winter, Phys. Rev. C **48**, 2524 (1993).
- [27] R. Schwengner, J. Döring, L. Funke, H. Rotter, G. Winter, A. Johnson, and A. Nilsson, Nucl. Phys. **A486**, 43 (1988).
- [28] L. Funke, J. Döring, P. Kemnitz, P. Ojeda, R. Schwengner, E. Will, G. Winter, A. Johnson, L. Hildingsson, and Th. Lindblad, Z. Phys. A **324**, 127 (1986).
- [29] J.W. Holcomb, J. Döring, T. Glasmacher, G.D. Johns, T.D. Johnson, M.A. Riley, P.C. Womble, and S.L. Tabor, Phys. Rev. C **48**, 1020 (1993).
- [30] J. Döring, R. Schwengner, L. Funke, H. Rotter, G. Winter, B. Cederwall, F. Lidén, A. Johnson, A. Atac, J. Nyberg, and G. Sletten, Phys. Rev. C **50**, 1845 (1994).
- [31] R. Schwengner, H. Schnare, S. Frauendorf, F. Dönau, L. Käubler, H. Prade, E. Grosse, A. Jungclaus, K.P. Lieb, C. Lingk, S. Skoda, J. Eberth, G. de Angelis, A. Gadea, E. Farnea, D.R. Napoli, C.A. Ur, and G. Lo Bianco, *ENAM 98, Exotic Nuclei and Atomic Masses*, edited by B.M. Sherrill, D.J. Morrissey and C.N. Davids, AIP Conf. Proc. No. 455 (AIP, Woodbury, NY, 1998), p. 594.
- [32] R. Schwengner, G. Winter, J. Reif, H. Prade, L. Käubler, R. Wirowski, N. Nicolay, S. Albers, S. Eßer, P. von Brentano, and W. Andrejtscheff, Nucl. Phys. **A584**, 159 (1995).
- [33] I. Ray, P. Banerjee, S. Bhattacharya, M. Saha-Sarkar, B. Sethi, J.M. Chatterjee, S. Chattopadhyay, A. Goswami, S. Muralithar, R.P. Singh, and R.K. Bhowmik, Nucl. Phys. **A646**, 141 (1999).
- [34] J. Eberth, Prog. Part. Nucl. Phys. **28**, 495 (1992).
- [35] D.C. Radford, Nucl. Instrum. Methods Phys. Res. A **361**, 297 (1995).
- [36] J. Theuerkauf, S. Esser, S. Krink, M. Luig, N. Nicolay, and H. Wolters, Program VS (version 6.65), Universität zu Köln, 1992 (unpublished).
- [37] R.M. Steffen, and K. Alder, in *The Electromagnetic Interaction in Nuclear Spectroscopy*, edited by W.D. Hamilton (North-Holland, Amsterdam, 1975), p. 505.
- [38] K.S. Krane, R.M. Steffen, and R.M. Wheeler, Nucl. Data Tables **11**, 351 (1973).
- [39] A. Krämer-Flecken, T. Morek, R.M. Lieder, W. Gast, G. Hebbinghaus, H.M. Jäger, and W. Urban, Nucl. Instrum. Methods Phys. Res. A **275**, 333 (1989).
- [40] L.P. Ekström and A. Nordlund, Nucl. Instrum. Methods Phys. Res. A **313**, 421 (1992).
- [41] J. Eberth, H.G. Thomas, D. Weißhaar, F. Becker, B. Fiedler, S. Skoda, P. von Brentano, C. Gund, L. Palafox, P. Reiter, D. Schwalm, D. Habs, T. Servene, R. Schwengner, H. Schnare, W. Schulze, H. Prade, G. Winter, A. Jungclaus, C. Lingk, C. Teich, and K.P. Lieb, Prog. Part. Nucl. Phys. **38**, 29 (1997).
- [42] G. Winter, Nucl. Instrum. Methods Phys. Res. **214**, 537 (1983).
- [43] J. Lindhard, V. Nielsen, and M. Scharff, Mat. Fys. Medd. K. Dan. Vidensk. Selsk. **36** (10), 1 (1968).
- [44] G. Winter, J. Döring, F. Dönau, and L. Funke, Z. Phys. A **334**, 415 (1989).
- [45] V.I. Dimitrov, F. Dönau, and S. Frauendorf, Phys. Rev. C **62**, 024315 (2000).
- [46] V.I. Dimitrov, S. Frauendorf, and F. Dönau, Phys. Rev. Lett. **84**, 5732 (2000).

- [47] R. Bengtsson, S. Frauendorf, and F.-R. May, *At. Data Nucl. Data Tables* **35**, 15 (1986).
- [48] A.A. Hecht, C.W. Beausang, K.E. Zyromski, D.L. Balabanski, C.J. Barton, M.A. Caprio, R.F. Casten, J.R. Cooper, D.J. Hartley, R. Krücken, D. Meyer, H. Newman, J.R. Novak, E.S. Paul, N. Pietralla, A. Wolf, N.V. Zamfir, Jing-Ye Zhang, and F. Dönau, *Phys. Rev. C* **63**, 051302(R) (2001).
- [49] D.J. Hartley, L.L. Riedinger, M.A. Riley, D.L. Balabanski, F.G. Kondev, R.W. Laird, J. Pfohl, D.E. Archer, T.B. Brown, R.M. Clark, M. Devlin, P. Fallon, I.M. Hibbert, D.T. Joss, D.R. LaFosse, P.J. Nolan, N.J. O'Brien, E.S. Paul, D.G. Sarantites, K. Sheline, S.L. Shepherd, J. Simpson, R. Wadsworth, Jing-ye Zhang, P.B. Semmes, and F. Dönau, *Phys. Rev. C* **64**, 031304 (2001).
- [50] T. Koike, K. Starosta, C.J. Chiara, D.B. Fossan, and D.R. LaFosse, *Phys. Rev. C* **63**, 061304(R) (2001).
- [51] K. Starosta, T. Koike, C.J. Chiara, D.B. Fossan, D.R. LaFosse, A.A. Hecht, C.W. Beausang, M.A. Caprio, J.R. Cooper, R. Krücken, J.R. Novak, N.V. Zamfir, K.E. Zyromski, D.J. Hartley, D. Balabanski, Jing-ye Zhang, S. Frauendorf, and V.I. Dimitrov, *Phys. Rev. Lett.* **86**, 971 (2001).